DOI: 10.1002/ejic.200800865

Heterometallic Ferrocene-Rhenium Complexes Linked by an Aminoethylglycine Scaffold

Lauren A. Levine,[a] Srećko I. Kirin,[a] Carl P. Myers,[a] Scott A. Showalter,[a] and Mary Elizabeth Williams*[a]

Keywords: Sandwich complexes / Ferrocene / Rhenium / Heterometallic complexes / Peptides

Using mono- and 1,*n*′-disubstituted ferrocenecarboxylic acid, the aminoethylglycine (aeg) derivatives Fe[C_5H_4-CO-aeg-O*t*Bu][C_5H_5] (**1**) and Fe[C_5H_4-CO-aeg-O*t*Bu]$_2$ (**2**) have been synthesized. Complexes **1** and **2** are further reacted to substitute the aeg with the nitrogen-containing ligands dpa-ph-CO_2H or py-AcOH to yield complexes **3**–**6**. Each of these is treated with $Re(CO)_5Cl$ to assemble heterometallic structures $\mathbf{3_{Re}}$–$\mathbf{6_{Re}}$. These are subsequently isolated and characterized by NMR and mass spectrometry, FTIR, UV/Vis absorbance, and fluorescence emission spectroscopy, and separately by electrochemistry. All of the compounds exhibit the characteristic redox properties of the ferrocene moiety; in the heterometallic compounds, an irreversible oxidative wave is attributed to the Re. The electrochemically determined diffusion coefficients of the compounds confirm that the as-prepared structures are discrete assemblies and not coordination polymers.

Introduction

Ferrocene (Fc)-containing compounds continue to be of intense interest due to their applications within catalysis[1] and materials science.[2] The geometry of Fc enables a variety of mono- and multi-metallic supramolecular structures to be synthesized,[3] and its well-known redox chemistry is desirable for use in conductive polymers and molecular electronics. A remaining challenge for construction of supramolecular systems is the specific relative placement of multiple inorganic species within the assembly. Recent work has focused on the synthesis of multi-component assemblies utilizing ferrocene as an electron donor either in simple dyads designed to create charge-separated states[4a,4b] or larger multi-component systems designed to generate NAD+ from NADH using proton-coupled electron transfer.[4c]

Our group is interested in building multi-metallic structures with applications for artificial photosynthesis[4] and photocatalysis.[5] Mimicking the molecular recognition of natural systems such as nucleic acids and proteins is one strategy for assembly of multi-metallic structures. For example, inorganic derivatives of DNA and peptide nucleic acid (PNA) have been successfully demonstrated.[6,7] Our previous work has reported the use of an aminoethylglycine (aeg) backbone with pendant heterocyclic ligands. Using these artificial peptides, we have shown that a variety of multimetallic structures can be assembled by coordinating transition-metal ions.[7] Illustrated in Figure 1 (A and B), traditional solid-phase peptide synthesis produces monomers with C and N termini, and therefore upon crosslinking leads to the formation of double-stranded parallel and antiparallel isomers. We have previously observed this with artificial oligopeptides in this group, and while that work illustrated using a peptide-based scaffold for molecular wires, further refinement of the molecular design to prevent isomer formation was clearly needed.

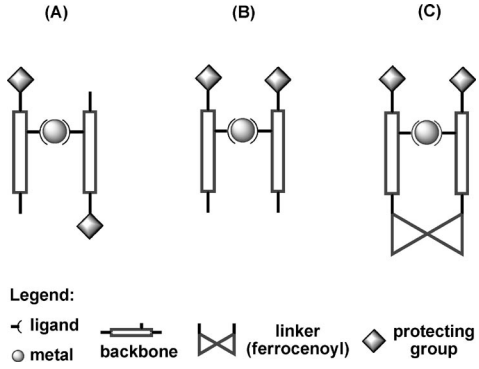

Figure 1. Structures of duplex isomers (**A**) and (**B**) and hairpin (**C**).

Inspiration from nucleic acid hairpin loops led us to design and build a "hairpin" geometry as shown in Figure 1 C; we first employed this motif using $Ru(bpy)_3^{2+}$ containing two ligand-decorated aeg monomers.[8] Addition of Cu^{2+} and Zn^{2+} formed coordinative crosslinks between the two

[a] Department of Chemistry, Pennsylvania State University, 104 Chemistry Building,
University Park, PA 16802, USA
E-mail: mbw@chem.psu.edu

Supporting information for this article is available on the WWW under http://www.eurjic.org or from the author.

aeg strands, self-assembling heterometallic structures. Mono- and di-functionalized ferrocenes (Fc) are alternative platforms for making mono and di-substituted loop structures. The well known redox chemistry of Fc makes it an attractive target for use in polymetallic molecular wires, diodes, and photoactive assemblies. We have therefore modified Fc with aeg strands that are substituted with pendant pyridine (py) or phenyl(dipyridyl)amine (dpa) ligands. The pendant ligands are subsequently reacted with pentacarbonylrhenium chloride[9] to form heterometallic assemblies linked by the aeg backbone.

In this article, we present the synthesis and characterization of aminoethyl-glycine (aeg)-substituted ferrocene artificial peptides and their heterometallic Re-containing complexes. The homo- and heterometallic compounds are characterized with NMR spectroscopy, high-resolution mass spectrometry, and FTIR spectroscopy. The UV/Vis spectroscopic and electrochemical properties are further examined. These Fc complexes serve as an alternative to the $Ru(bpy)_3^{2+}$-based complexes, and demonstrate that the "hairpin" motif is more generally applicable for making heterofunctional and redox-active inorganic structures.

Results and Discussion

Synthesis

We have synthesized and characterized ferrocene complexes containing modified aeg. Mono-substituted ferrocenoyl **1**, **3** and **5** were prepared according to the method shown in Scheme 1. Standard amide-coupling conditions were used and **1** was isolated in 82% yield. Complex **1** was further treated with dpa-ph-CO_2H or with the commercially available pyridylacetic acid to give the ligand-substituted derivatives **3** (81% yield) and **5** (58% yield), respectively.

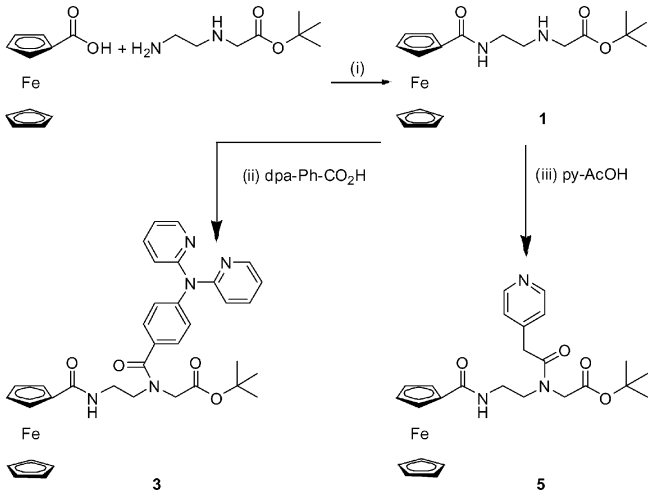

Scheme 1. Synthesis of **1**, **3** and **5**. Reaction conditions: (i) – (iii) HBTU/HOBt·H_2O/DIPEA/CH_2Cl_2/0 °C → r.t./16 h; yield (i) 82%, (iii) 58%, (ii) 81%.

The syntheses of di-substituted ferrocenoyl complexes **2**, **4** and **6** are depicted in Scheme 2. These reactions are analogous to those described in Scheme 1 for the mono-substituted **1**, **3** and **5** with the exception that the reactions in

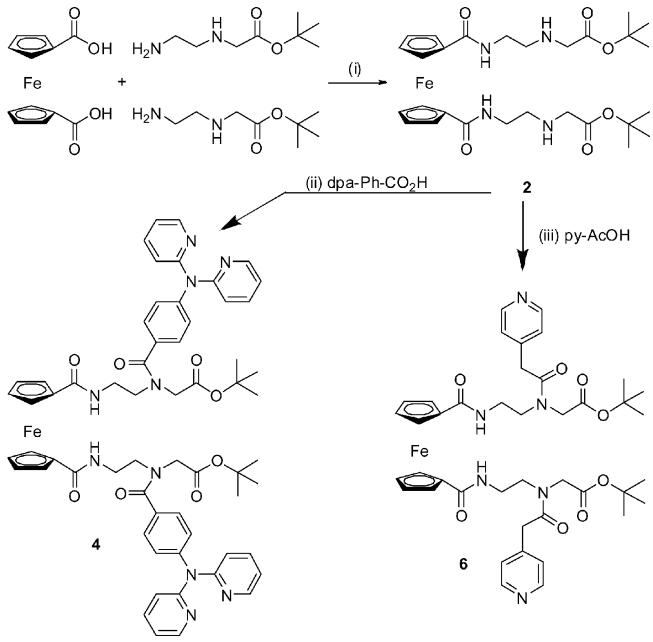

Scheme 2. Synthesis of **4**–**6**. Reaction conditions: (i) – (iii) HBTU/HOBt·H_2O/DIPEA/CH_2Cl_2/0 °C → r.t.; yield (i) 71%, (ii) 83% and (iii) 98%.

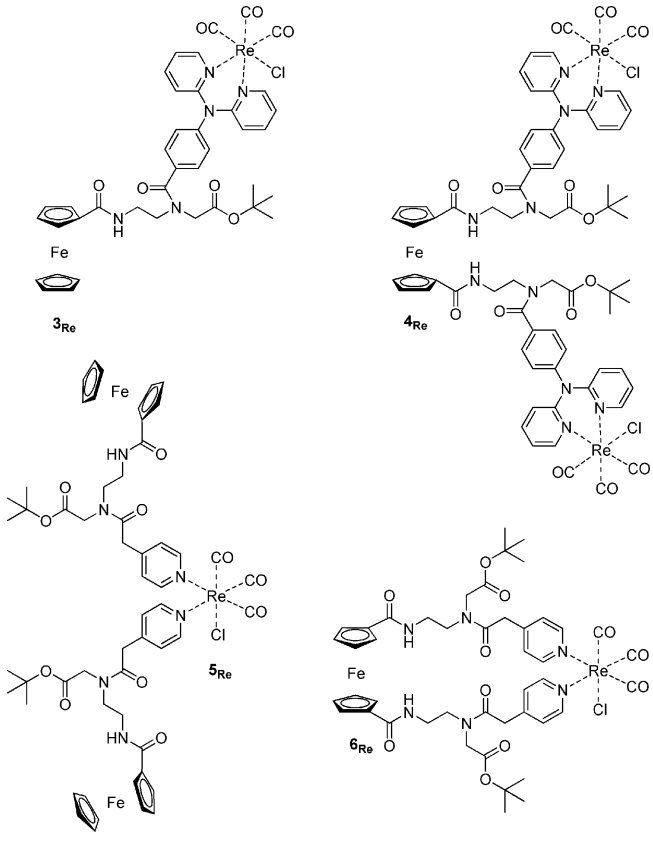

Figure 2. Structures of heterometallic complexes $\mathbf{3_{Re}}$–$\mathbf{6_{Re}}$.

Scheme 2 require longer reaction times and double coupling (i.e., using additional equivalents of the acid or amine) to proceed with high yields (71–98%).

The heterometallic complexes $\mathbf{3_{Re}}$–$\mathbf{6_{Re}}$ have been prepared by refluxing the corresponding ferrocenoyl complexes **3**–**6** with $Re(CO)_5Cl$ in chloroform.[10] As a result, two carbonyl ligands in the $Re(CO)_5Cl$ precursor are substituted with one bidentate dpa in $\mathbf{2_{Re}}$ and $\mathbf{3_{Re}}$ or with two monodentate pyridine moieties in $\mathbf{5_{Re}}$ and $\mathbf{6_{Re}}$ (Figure 2). After purification by column chromatography on silica, $\mathbf{3_{Re}}$–$\mathbf{6_{Re}}$ were isolated in 53–65% yield.

Characterization

Ferrocene compounds **1**–**6** and heterometallic complexes $\mathbf{3_{Re}}$–$\mathbf{6_{Re}}$ were characterized by high-resolution time-of-flight positive-ion electrospray (TOF-ES+) mass spectrometry. All mass spectra contain a strong molecular ion peak $[M + H]^+$ with the predicted isotopic pattern for the targeted product. Complexes $\mathbf{3_{Re}}$–$\mathbf{6_{Re}}$ were further characterized by FTIR spectroscopy; selected regions of the FTIR spectra of these compounds are shown in Figure 3 (for full spectra, see Supporting Information). The CO stretching bands are observed as three peaks of similar intensity in the region between 2050 and 1850 cm^{-1}. This pattern is expected for the *fac*-isomer of the CO groups on the Re (the *mer*-isomer would reveal three peaks with significantly different intensities,[9c,11] confirming the structural environment around each Re center).

In ^1H NMR spectra, the presence of amide proton resonances above 7 ppm in non-hydrogen-bonding solvents like $CDCl_3$ is indicative of hydrogen bonding. In the case of mono-substituted derivative **1**, the amide proton is observed below 7 ppm, consistent with a lack of hydrogen bonding. Conversely, the amide protons of the resulting ferrocenoyl peptidic analogs are found above 7 ppm, suggesting hydrogen bonding between the two aeg strands as has been reported in closely related 1,*n*′-disubstituted ferrocenoyl peptides.[12] After the introduction of the $Re(CO)_3Cl$ moiety in $\mathbf{3_{Re}}$–$\mathbf{6_{Re}}$, the ^1H NMR spectra of the corresponding free $\mathbf{3_{Re}}$–$\mathbf{6_{Re}}$ show significant changes (as shown in Supporting Information). Shifts in the pendant ligands as well as amide peaks are observed upon metal binding with larger shifts ($\Delta\delta$ = 0.2–0.7) for $\mathbf{3_{Re}}$ and $\mathbf{4_{Re}}$ and smaller shifts ($\Delta\delta$ = 0.05–0.28) for $\mathbf{5_{Re}}$ and $\mathbf{6_{Re}}$. In contrast, the ferrocenoyl ^1H peaks show no noticeable shifts following coordination of the Re metals.

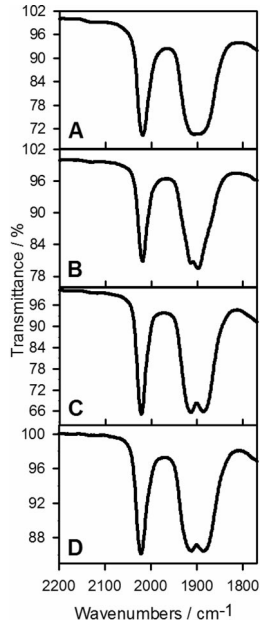

Figure 3. FTIR spectra of A) $\mathbf{3_{Re}}$, B) $\mathbf{4_{Re}}$, C) $\mathbf{5_{Re}}$, D) $\mathbf{6_{Re}}$.

Using the variation ratio method, the chemical shifts of the amide protons are compared in a non-coordinating solvent ($CDCl_3$) and a coordinating solvent ($[D_6]DMSO$).[13] These shifts are compared to a standard compound (**1**) which possesses NH groups in a comparable chemical environment but which does not hydrogen bond. The chemical shift variation from $[D_6]DMSO$ to $CDCl_3$ for each compound is determined ($\Delta\delta_{NH}$). The extent of hydrogen bonding can be determined by comparing the ratio of the $\Delta\delta$ values; for compounds **2** to **6** and their heterometallic counter-parts, these are compared with $\Delta\delta$ for compound **1**. The difference is reported as the variation ratio (vr) = $\Delta\delta_{substrate}/\Delta\delta_{reference}$. Larger values of vr correspond to weaker hydrogen bonding in the molecule. In Table 1, the di-substituted homometallic ferrocenoyl peptides have vr values of ca. 0.27 and therefore have stronger hydrogen bonding. Both the mono-substituted and heterometallic complexes have larger vr values (0.5–0.7), indicating that these have weaker hydrogen bonding.

Table 1. ^1H NMR spectroscopic data.

	δ_{NH} /ppm in $CDCl_3$	δ_{NH} /ppm in $[D_6]DMSO$	$\Delta\delta$ /ppm $\delta_{[D6]DMSO} - \delta_{CDCl3}$	$vr = \Delta\delta_{substrate}/\Delta\delta_{standard}$ (standard)	k_{ex} /s^{-1} in CD_3CN
1	6.49	7.75	1.26	1.00	
2	7.54	7.87	0.33	0.26	
3	7.2	7.91	0.71	0.56	22.0 ± 1.0
4	7.65	7.99	0.34	0.27	36.4 ± 1.8
5	7.24	7.96	0.72	0.57	4.4 ± 0.2
6	7.67	8.03	0.36	0.29	18.8 ± 0.9
$\mathbf{3_{Re}}$	7.04	7.92	0.88	0.70	14.5 ± 0.7
$\mathbf{4_{Re}}$	7.03	7.89	0.86	0.68	24.5 ± 1.2
$\mathbf{5_{Re}}$	7.19	7.95	0.76	0.60	5.7 ± 0.3
$\mathbf{6_{Re}}$	7.39	8.04	0.65	0.52	26.4 ± 1.3

Analysis of the room-temperature ^{1}H NMR spectra also revealed the presence of slow conformational exchange in both the mono- and di-substituted peptides. This is demonstrated for the Fc region of the compound **3** spectrum (Figure 4), where several pairs of peaks clearly resolved at low temperatures are seen to coalesce as the temperature (and therefore exchange rate) is elevated. Identical variable-temperature experimental data were acquired for compounds **3**–**6** and $\mathbf{3_{Re}}$ – $\mathbf{6_{Re}}$, revealing the temperature-dependent rate of interconversion (k_{ex}) between the two conformers. At room temperature (295 K, consistent with the electrochemistry experiments), k_{ex} ranged from 4.40 to 36.4 s^{-1} (summarized in Table 1); with the exchange constant largely insensitive to the addition of Re metals. Although k_{ex} is similar for all compounds at 295 K, the rise in k_{ex} with increasing temperature is systematically greater for the dpa-containing compounds than for their pyridyl-substituted equivalents, suggesting lower activation energy for the conformational change in the dpa-containing compounds.

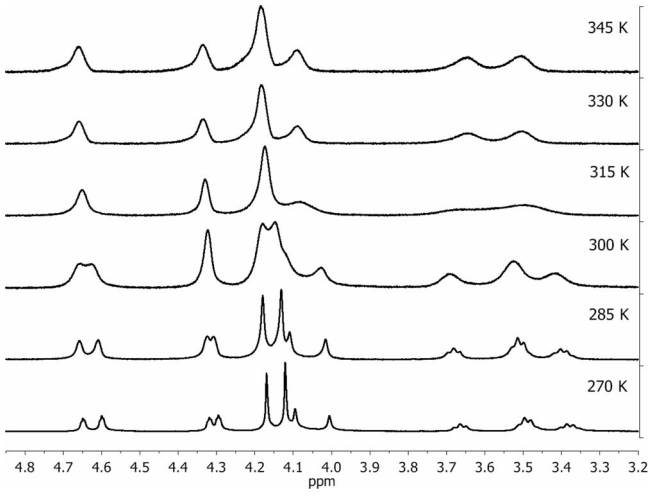

Figure 4. Variable-temperature ^{1}H NMR of compound **3**.

Electronic Spectroscopy

The UV/Vis absorbance spectra for the single-stranded complexes are shown in Figure 5 and for the double-stranded complexes in Figure 6. These data are summarized in Table 2. All complexes possess a characteristic low inten-

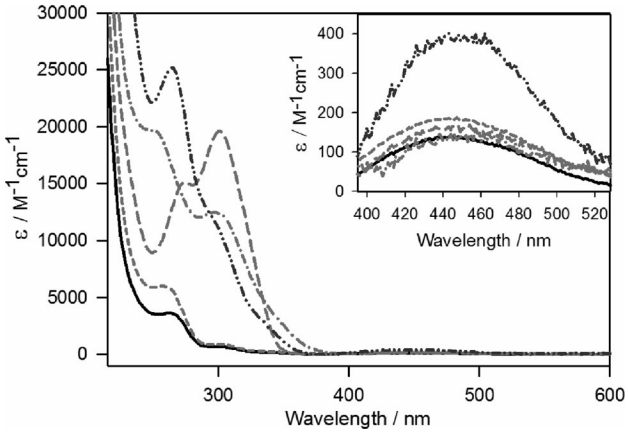

Figure 5. Absorbance spectra of **1** (–), **3** (—), **5** (– –), $\mathbf{3_{Re}}$ (–·–), and $\mathbf{5_{Re}}$ (–··–) in acetonitrile. Inset: expanded region of the spectra.

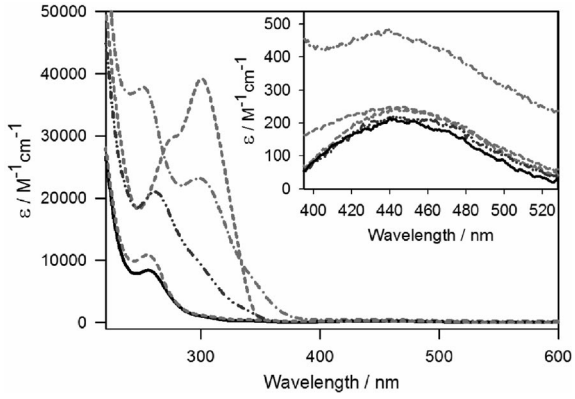

Figure 6. Absorbance spectra of **2** (–), **4** (—), **6** (– –), $\mathbf{4_{Re}}$ (–·–), and $\mathbf{6_{Re}}$ (–··–) in acetonitrile. Inset: expanded region of the spectra.

Table 2. Compilation of physical data.

	λ_{abs} /nm [$\varepsilon \times 10^3$ /M^{-1} cm^{-1}][a]	$\lambda_{em,max}$ /nm [Φ][b]	$Fc^{+/0}$ E^o /V[c] [ΔE_p /mV][d]	$Re^{II/I}$ E^o /V[c]	D ($\times 10^{-5}$) /cm^2 s^{-1}[e]
1	263 [3.96], 302 [0.76], 336[f] [0.21], 444[g] [0.16]		0.47 [60]		1.30
2	256 [8.11], 343[f] [0.34], 444[g] [0.21]		0.72 [84]		1.20
3	275 [16.21], 300 [20.39], 447[g] [0.17]	401 [0.027]	0.46 [72]		0.96
4	275 [29.80], 300 [38.88], 447[g] [0.23]	384 [0.013]	0.64 [78]		0.72
5	262 [6.14], 302 [0.97], 342[f] [0.29], 444[g] [0.20]		0.48 [74]		1.16
6	257 [11.1], 348[f] [0.30], 444[g] [0.21]		0.69 [96]		0.83
$\mathbf{3_{Re}}$	254 [19.00], 300 [12.69], 440[g] [0.16]	394 [>0.01]	0.47 [66]	1.35	0.63
$\mathbf{4_{Re}}$	252 [48.53], 300 [29.49], 440[g] [0.30]	392 [>0.01]	0.69 [66]	1.36	0.54
$\mathbf{5_{Re}}$	265 [24.24], 302[f] [10.88], 444[g] [0.39]		0.47 [72]	1.42	0.77
$\mathbf{6_{Re}}$	262 [20.25], 302[f] [9.20], 444[g] [0.22]		0.63 [78]	1.39	0.80

[a] The absorption spectra were measured in acetonitrile. [b] Emission spectra were measured in acetonitrile in dearated solutions. [c] Formal potential measured as the average peak potential for the reaction in V vs. SCE. [d] Differences in the cathodic and anodic potentials in the cyclic voltammogram, measured at a potential scan rate of 50 mV/s. [e] Diffusion coefficient calculated from the slopes of the Cottrell plots from chronoamperometry and analyzed using Equation (1). [f] Shoulder. [g] Broad peak.

sity (ε = 140–400 $M^{-1}cm^{-1}$) band with maxima at ca. 440 nm that is assigned to the d–d* transition of the ferrocene moiety.[14] The dpa-containing complexes **3** and **4** possess a strong absorbance band (ε = 16,000–38,600 $M^{-1}cm^{-1}$) with maxima at 300 nm, which is assigned to the ligand-centered π–π* transition, and a shoulder at 252–265 nm that is assigned as a pyridine-centered ligand-centered transition.[15] The heterometallic dpa-substituted complexes $\mathbf{3}_{Re}$ and $\mathbf{4}_{Re}$ have distinctly different electronic absorption spectra: the peak centered at 300 nm is still present but at lower intensity, and there is also a 20 nm blue shift and an increase in absorptivity of a shoulder with higher energy. The metal ligand charge-transition band is much weaker and only appears as a tail toward the visible region.[9,16] In the case of the pyridyl-substituted complexes **5** and **6**, absorbance at 260 nm is due to a pyridine-centered π–π* transition. With the addition of Re to compounds **5**–**6**, an increase in the extinction coefficient of the py-ligand-centered π–π* transition is observed. Similarly, there is an increase in the extinction coefficient in $\mathbf{5}_{Re}$ for the Fc d–d* transition because the molecule contains two bound Fc moieties.

In thoroughly dearated solutions, excitation of all dpa-containing molecules at the π–π* transition for the dpa-ph-OH ligand (λ_{ex} = 325 nm) gives rise to the emission spectra shown in Figure 7. These contain a single peak that is attributed to the relaxation of a ligand-centered excited state with quantum yields of 0.027 and 0.013 for **3** and **4**, respectively. Because it is known that dpa emission is quenched at high solution concentrations, the lower quantum yield for **4** may be due to the high local concentration caused by tethering the ligands within the same species. In comparison with the dpa ligand (i.e. not bound to Fc), the much lower fluorescence quantum yields are indicative of a high degree of quenching by the proximal ferrocene moiety.[17] This observation is consistent with excited state quenching by either energy transfer or electron transfer from the Fc to the dpa*.[17] Similar to prior reports of Re(dpa) complexes, emission of the dpa ligand is further quenched upon the chelation of Re;[16] complexes $\mathbf{3}_{Re}$ and $\mathbf{4}_{Re}$ each have quantum yields that are less than 1%.

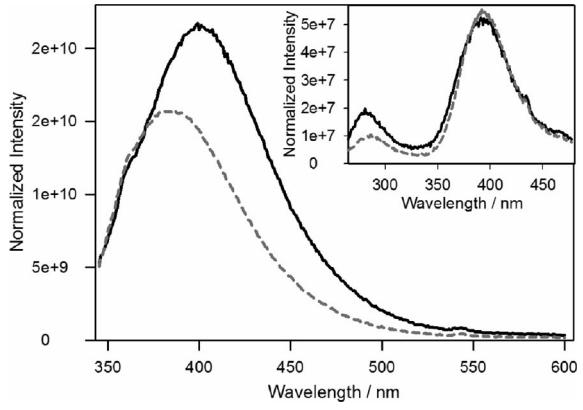

Figure 7. Emission spectra for compounds 5.6 μM **3** (–), 9.5 μM **4** (– –) in deaerated acetonitrile solutions following excitation at λ_{ex} = 325 nm. Spectra are normalized to concentration using the known extinction coefficient of each complex. Inset: normalized emission spectra of 186.2 μM $\mathbf{3}_{Re}$ (–), 245.1 μM $\mathbf{4}_{Re}$ (– –) in deaerated acetonitrile solutions following excitation at λ_{ex} = 245 nm.

Electrochemistry

Because the oxidative electrochemistry of Fc is well known, electrochemical experiments were further employed to characterize the Fc aeg-substituted complexes. Cyclic voltammetry was used to measure the redox potentials of each of the ferrocenoyl complexes; the voltammograms are shown in Figure 8 and data summarized in Table 2. The single-stranded Fc-functionalized peptides **1**, **3**, and **5** have a positive shift in the formal potential (E^o) by ca. 200 mV relative to unsubstituted Fc.[3,18,19] The complexes substituted with two artificial peptides **2**, **4**, and **6** exhibit a larger shift in the formal potential (≈ 400 mV).[17,20] In all cases the oxidative reactions are electrochemically quasi-reversible with ΔE_p of 60–84 mV. The single-stranded heterometallic complexes $\mathbf{3}_{Re}$ and $\mathbf{5}_{Re}$ exhibit Fc-centered oxidations at potentials that are essentially the same as the homo-metallic structures. These additionally have a chemically irreversible oxidation at E^o at 1.35 and 1.42 V for $\mathbf{3}_{Re}$ and $\mathbf{5}_{Re}$, respectively, which is due to oxidation of the Re.[21] A similar oxidation wave is observed in the cyclic voltammograms for the double-stranded oligopeptides at E^o at 1.36 and 1.39 V for $\mathbf{4}_{Re}$ and $\mathbf{6}_{Re}$.

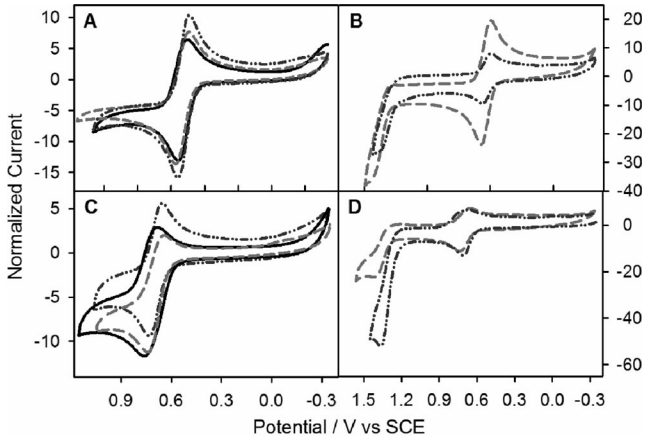

Figure 8. Cyclic voltammograms in deaerated ACN solutions containing 0.2 M TBAP supporting electrolyte. Current is normalized for concentration. Potential scan rate was 50 mV/s. A: **1** (–), **3** (–··–), and **5** (– –). B: $\mathbf{3}_{Re}$ (–··–), $\mathbf{5}_{Re}$ (– –). C: **2** (–), **4** (–··–), and **6** (– –). D: $\mathbf{4}_{Re}$ (–··–), $\mathbf{6}_{Re}$ (– –).

The diffusion coefficients of each of the species are determined using potential-step chronoamperometry. For each compound, a potential step is applied by stepping to the mass-transport limited region of the wave (determined from the cyclic voltammograms, at least 100 mV more positive of the formal potential for the $Fc^{0/1+}$), and the current (i) is monitored as a function of time. Figure 9 shows the plots of linearized current transient acquired during the chronoamperometric experiments. For both the homo- and heterometallic complexes, the linearity of the plots indicates

that the oxidation reaction is diffusion-limited. These data are quantitatively analyzed using the well-known Cottrell equation (1).[18]

$$i = \frac{nFAD^{1/2}C}{\pi^{1/2}t^{1/2}} \quad (1)$$

where n is the number of electrons in the reaction (n = 1); F is the Faraday constant, A is the surface area of the working electrode; D is the diffusion coefficient; and C is the concentration of the complex. The slopes of the lines in Figure 9 were therefore used to calculate the diffusion coefficients for each complex. Values of D for the homometallic complexes are listed in Table 2. In all cases, the mass-transport rate (e.g., D) decreases as the size of the redox-active species increases: dpa-substituted artificial peptides having smaller diffusion coefficients than their py counterparts.[22]

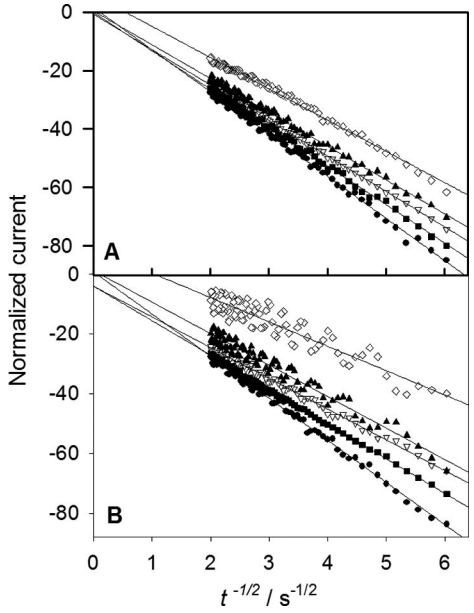

Figure 9. Plots of the linearized current-time transients for A: **1** (●), **3** (∇), **5** (■), $\mathbf{3_{Re}}$ (✧), and $\mathbf{5_{Re}}$ (▲) resulting from applied potential steps from E = 0 V to E = 0.80 V, 0.80 V, 0.90 V, 0.73 V and 1.1 V for **1**, **3**, **5**, $\mathbf{3_{Re}}$, and $\mathbf{5_{Re}}$, respectively; and for B: **2** (●), **4** (∇), **6** (■), $\mathbf{4_{Re}}$ (✧), and $\mathbf{6_{Re}}$ (▲) resulting from applied potential step from E = 0 V to E = 1.05 V, 0.94 V, 1.05 V, 0.55 V, 0.90 V for **2**, **4**, **6**, $\mathbf{4_{Re}}$, and $\mathbf{6_{Re}}$, respectively. Currents are normalized to concentration.

Conclusion

A series of new heterometallic complexes $\mathbf{3_{Re}}$–$\mathbf{6_{Re}}$ is prepared, and characterized by MS, FTIR, UV/Vis, fluorescence, electrochemistry and NMR spectroscopy. The dpa-substituted Fc compounds (**3** and **4**) are shown to be luminescent until used for heterometallic complexes. For all compounds, the diffusion coefficients determined using the $Fc^{0/1+}$ couple are consistent with the formation of the structures shown in Figure 2 vs. coordination polymers. All four heterometallic complexes, $\mathbf{3_{Re}}$–$\mathbf{6_{Re}}$, have C-terminal ends that allow the construction of Re-derived aeg-oligomers via amide-coupling procedures. Our current efforts are focused on chain elongation and self-assembly of larger, redox and photoactive multimetallic structures.

Experimental Section

Chemicals: $ReCO_5Cl$ was purchased from Strem. All other materials were purchased from either Sigma–Aldrich or VWR and used as received unless otherwise noted. Chemicals were used without further purification except where indicated. Dichloromethane and tetrahydrofuran (THF) were dried by passing through a column with activated alumina. For all experiments, ultrapure water was used (Labconco Water Pro PS system, 18.2 MΩ).

Instrumentation and Analysis: Positive-ion electrospray mass spectrometry (ESI^+) was performed at the Penn State Mass Spectrometry Facility using a Mariner mass spectrometer (Perseptive Biosystems). All NMR spectra were collected with a Bruker Avance 360 MHz spectrometer. For the variable-temperature studies, samples were maintained at 270–345 K in intervals of 5 K, with a delay of > 15 min at each temperature prior to acquisition to ensure sample-temperature equilibration. Studies were performed using standard one-pulse-proton NMR experiments. Temperature was ramped up from 270 K to 345 K and then back down to 270 K to test for hysteresis. CD_3CN was empirically determined to be the best solvent for the variable temperature studies as exchange became negligible for all compounds by 270 K and peak coalescence was observed for most samples by 345 K, which is safely below the boiling point of the solvent. All data were fit to a simple two-site exchange model.[23] ^{13}C NMR spectra were collected with a Bruker Avance 400 MHz spectrometer. Coupling constants are given in Hz.

The UV/Vis absorbance spectra were obtained with a double-beam spectrophotometer (Varian, Cary 500) using a 1-cm quartz cuvette in HPLC-grade acetonitrile. Steady-state emission experiments were performed using a 1-cm quartz cuvette at room temperature using a PTI Photon Technology Instruments equipped with an 814 photomultiplier detector. Quantum-efficiency measurements were carried out at room temperature in HPLC-grade acetonitrile. Samples were measured in deaerated solutions following literature methods.[24] Solutions of deaerated $Ru(bpy)_3^{2+}$ (Φ = 0.062) in acetonitrile and anthracene (Φ = 0.27) in ethanol were used as references. Diffuse reflectance IR spectra were measured with a Varian FTS 7000 spectrometer in KBr pellets.

Electrochemistry: All electrochemical measurements were obtained using a CH Instruments potentiostat (Model 660) with a 0.31-cm diameter glassy-carbon working and Pt-wire counter electrodes with a Ag/Ag^+ reference electrode. Solutions were prepared from distilled ACN containing 0.2 M tetra-*n*-butylammonium perchlorate (TBAP, recrystallized three times) supporting electrolyte. The solutions were prepared, stored, and analyzed under N_2. Reported redox potentials are based on the observed peak potentials in the cyclic voltammograms, and are converted into the saturated calomel electrode (SCE) scale using a ferrocene/ferrocenium (Cp_2Fe/Cp_2Fe^+) internal standard.[18] Chronoamperometric measurements were corrected for background currents by subtracting the current transients obtained from potential steps of equal magnitude to solutions containing solely supporting electrolyte.

Synthesis: *tert*-Butyl *N*-(aminoethyl)glycinate (aeg-O-*tert*-butyl)[25] and 4-[bis(pyrid-2-yl)amino]benzoic acid (dpa-ph-CO_2H)[26] was synthesized as previously reported.

Ferrocenoyl Complexes 1–6. General Procedure: The corresponding carboxylic acid (1 equiv.) was suspended in dichloromethane and cooled to 0 °C in an ice bath. HBTU (1 equiv.), HOBt·H_2O (1 equiv.) and DIPEA (4 equiv.) were added. After the clear solution was stirred for 1 h at 0 °C, the amine (1 equiv.) was added. The reaction mixture was allowed to reach room temperature, and stirring continued for the indicated period. The reaction mixture was then washed with satd. aqueous sodium hydrogen carbonate. The orange organic extracts were dried with sodium sulfate, filtered and evaporated under reduced pressure to obtain the crude product that was purified as indicated bellow.

Fe[C_5H_4-CO-aeg-O*t*Bu][C_5H_5] (1): Ferrocenecarboxylic acid (0.73 g, 2.5 mmol), dichloromethane (100 mL), HBTU (0.95 g, 2.5 mmol), HOBt·H_2O (383 mg, 2.5 mmol), DIPEA (1.7 mL, 10 mmol) and H-aeg-O*t*Bu (0.44 g, 2.5 mmol) were reacted for 20 h. After the reaction mixture was washed with sodium hydrogen carbonate (satd. aq., 3 × 80 mL), the organic layer was extracted with citric acid (10% aq., 3 × 80 mL). The orange acidic extracts were neutralized with solid sodium hydrogen carbonate and extracted with dichloromethane (3 × 80 mL). The combined organic extracts were dried (Na_2SO_4), filtered and evaporated under reduced pressure to yield an orange-red viscous oil that solidifies upon standing (0.92 g, 82%). The crude product was used for the next step without further purification. An analytical sample was obtained by flash column chromatography (silica, 0 → 10% MeOH in EtOAc). HR-MS (TOF ES+): *m*/*z* exp. 387.1345 and calcd. 387.1371 for [M + H]$^+$. ^{1}H NMR ($CDCl_3$): δ = 6.52 (m, 1 H, H_{NH}), 4.71 (br. s, 2 H, $H_{Fc-\alpha}$), 4.32 (br. s, 2 H, $H_{Fc-\beta}$), 4.20 (s, 5 H, $H_{Fc-unsubst.}$), 3.46–3.40 (m, 2 H, H_{Bb-2}), 3.34 (s, 2 H, H_{Bb-5}), 2.83 (t, *J* = 5.6 Hz, 2 H, H_{Bb-3}), 1.71 (br. s, 1 H, H_{Bb-4}), 1.48 (s, 9 H, H_{OtBu}) ppm. ^{13}C NMR ($CDCl_3$): δ = 172.17 (CO_{ester}), 170.35 (CO_{amide}), 81.44 (C_{tBu-q}), 76.36 (C_{Fc-i}), 70.21 ($C_{Fc-\alpha}$), 69.66 (2 C, $C_{Fc-unsubst.}$), 68.14 ($C_{Fc-\beta}$), 51.10 (C_{Bb-5}), 48.58 (C_{Bb-3}), 38.97 (C_{Bb-2}), 28.09 (Ct_{Bu-Me}) ppm.

Fe[C_5H_4-CO-aeg-O*t*Bu]$_2$ (2): Ferrocenedicarboxylic acid (548 mg, 2.0 mmol), dichloromethane (80 mL), HBTU (758 mg, 2.0 mmol), HOBt·H_2O (305 mg, 2.0 mmol), DIPEA (1.4 mL, 8 mmol) and H-aeg-O*t*Bu (435 mg, 2.5 mmol) were combined, and the reaction mixture stirred at room temperature for 20 h. Additional HBTU (758 mg, 2.0 mmol), HOBt·H_2O (305 mg, 2.0 mmol), DIPEA (1.4 mL, 8 mmol) and H-aeg-O*t*Bu (435 mg, 2.5 mmol) were added and the reaction was continued for another 20 h. The crude product was purified by column chromatography (silica, EtOAc/EtOH, 1:1). Yield 0.83 g (71%) of orange foam. HR-MS (TOF ES+): *m*/*z* exp. 587.2523 and calcd. 587.2532 for [M + H]$^+$. ^{1}H NMR ($CDCl_3$): δ = 7.57 (m, 2 H, H_{NH}), 4.58 (br. s, 4 H, $H_{Fc-\alpha}$), 4.39 (br. s, 4 H, $H_{Fc-\beta}$), 3.49–3.44 (m, 4 H, H_{Bb-2}), 3.35 (s, 4 H, H_{Bb-5}), 2.90 (t, *J* = 5.6 Hz, 4 H, H_{Bb-3}), 1.85 (br. s, 1 H, H_{Bb-4}), 1.44 (s, 18 H, H_{OtBu}) ppm. ^{13}C NMR ($CDCl_3$): δ = 171.41 (CO_{ester}), 170.13 (CO_{amide}), 81.69 (Ct_{Bu-q}), 77.51 (C_{Fc-i}), 71.20 ($C_{Fc-\alpha}$), 70.52 ($C_{Fc-\beta}$), 51.23 (C_{Bb-5}), 48.81 (C_{Bb-3}), 39.33 (C_{Bb-2}), 28.02 (Ct_{Bu-Me}) ppm.

Fe[C_5H_4-CO-aeg(dpa-ph)-O*t*Bu][C_5H_5] (3): dpa-ph-CO_2H (0.29 g, 1.0 mmol), dichloromethane (30 mL), HBTU (0.38 mg, 1.0 mmol), HOBt·H_2O (153 mg, 1.0 mmol), DIPEA (1.05 mL, 10 mmol) and ferrocenoyl mono-backbone **1** (235 mg, 0.6 mmol) were combined, and the reaction mixture stirred at room temperature for 48 h. An additional Dpa-ph-CO_2H (291 mg, 1.0 mmol), dichloromethane (30 mL), HBTU (379 mg, 1 mmol), HOBt·H_2O (153 mg, 1.0 mmol) and DIPEA (1.05 mL, 10 mmol) were added and the reaction was continued for another 48 h. The crude product was purified by column chromatography (silica, 0 → 10% MeOH in EtOAc). Yield 0.32 mg (81%) of orange solid. HR-MS (TOF ES$^+$): *m*/*z* exp. 660.2245 and calcd. 660.2273 for [M + H]$^+$. ^{1}H NMR ([D_6]-DMSO), max./min. where observed: δ = 8.26 (br. s., 2 H, H_{py-6}), 7.91–7.87 (br. m, 1 H, NH), 7.71 (t, *J* = 7.5 Hz, 2 H, H_{py-4}), 7.38/7.32 (d, *J* = 7.5 Hz, 2 H, $H_{ph-3,5}$), 7.10–6.96 (m, 6 H, $H_{ph-2,6}$, H_{py-3} and H_{py-5}), 4.71/4.76 (br. s, 2 H, $H_{Fc-\beta}$), 4.33 (br. s, 2 H, $H_{Fc-\beta}$), 4.11/4.16 (s, 5 H, $H_{Fc-unsubst.}$), 3.69–3.38 (m, 6 H, H_{Bb-2}, H_{Bb-4} and H_{Bb-5}), 1.45/1.36 (s, 9 H, H_{OtBu}), max./min. ratio 58:42.

Fe[C_5H_4-CO-aeg(dpa-ph)-O*t*Bu]$_2$ (4): Dpa-ph-CO_2H (0.29 g, 1.0 mmol), dichloromethane (30 mL), HBTU (0.38 g, 1.0 mmol), HOBt·H_2O (0.15 g, 1.0 mmol), DIPEA (1.05 mL, 10 mmol) and ferrocenoyl bis-backbone **2** (0.19 g, 0.32 mmol) were combined and the reaction mixture stirred at room temperature for 72 h. The crude product was purified by column chromatography (silica, EtOAc/EtOH, 1:1). Yield 300 mg (83%) of orange foam. HR-MS (TOF ES+): *m*/*z* = exp. 1133.4346 and calcd. 1133.4336 for [M + H]$^+$. ^{1}H NMR ([D_6]DMSO) max./min. where observed: δ = 8.25 (d, *J* = 4.0 Hz, 2 H, H_{Py-6}), 8.05–7.92 (br. s, 1 H, H_{NH}), 7.69 (dt and 7.5, *J* = 1.7 Hz, 2 H, H_{py-4}), 7.37–7.27 (br. s, 2 H, $H_{ph-3,5}$), 7.09–6.98 (m, 6 H, $H_{ph-2,6}$, H_{py-3} and H_{py-5}), 4.72–4.65 (m, 2 H, $H_{Fc-\alpha}$), 4.29–3.94 (m, 4 H, H_{Fc-b} and H_{Bb-5}), 3.60–3.41 (m, 4 H, H_{Bb-2} and H_{Bb-3}), 1.44/1.34 (s, 9 H, H_{OtBu}), max./min. 60:40.

Fe[C_5H_4-CO-aeg(py)-O*t*Bu][C_5H_5] (5): 4-Pyridinecarboxylic acid (260 mg, 1.5 mmol), dichloromethane (60 mL), HBTU (569 mg, 1.5 mmol), HOBt·H_2O (230 mg, 1.5 mmol), DIPEA (1.05 mL, 10 mmol) and ferrocenoyl mono-backbone **1** (579 mg, 1.5 mmol) were combined and allowed to react for 48 h. The crude product was purified by column chromatography (silica, 0 → 10% MeOH in EtOAc). Yield 440 mg (58%) of orange-red viscose oil. HR-MS (TOF ES+): *m*/*z* exp. 506.1733 and calcd. 506.1742 for [M + H]$^+$. ^{1}H NMR ([D_6]DMSO) max./min. where observed: δ = 8.48–8.47 (m, 2 H, $H_{py-2,6}$), 7.95–7.94/7.78–7.77 (m, 1 H, H_{NH}), 7.28–7.26/7.22–7.21 (m, 2 H, $H_{py-3,5}$), 4.79/4.73 (br. s, 2 H, $H_{Fc-\alpha}$), 4.37/4.34 (br. s, 2 H, $H_{Fc-\beta}$), 4.15 (br. s, 5 H, $H_{Fc-unsubst.}$), 4.00/4.28 (br. s, 2 H, $H_{Py-\alpha}$), 3.86/3.67 (br. s, 2 H, H_{Bb-5}), 3.48–3.38 (m, 4 H, H_{Bb-2} and H_{Bb-3}), 1.38/1.41 (s, 9 H, H_{OtBu}), max./min. ratio 68:32.

Fe[C_5H_4-CO-aeg(py)-O*t*Bu]$_2$ (6): 4-Pyridinecarboxylic acid (0.374 g, 1.65 mmol), dichloromethane (20 mL), HBTU (0.610 g, 1.65 mmol), HOBt·H_2O (306 mg, 1.6 mmol), DIPEA (1.4 mL, 8.0 mmol) and ferrocenoyl bis-backbone **2** (0.48 g, 0.82 mmol) were used and the reaction mixture was stirred at room temperature for 24 h. Additional 4-pyridinecarboxylic acid (0.374 g, 1.65 mmol), dichloromethane (20 mL), HBTU (0.610 g, 1.65 mmol), HOBt·H_2O (0.31 g, 1.6 mmol), DIPEA (1.4 mL, 8 mmol) were added and the reaction was continued for another 24 h. Additional 4-pyridinecarboxylic acid (0.374 g, 1.65 mmol), dichloromethane (20 mL), HBTU (0.610 g, 1.65 mmol), HOBt·H_2O (0.31 g, 1.6 mmol), DIPEA (1.4 mL, 8.0 mmol) were added and the reaction continued for the third time for 24 h. The crude product was purified by column chromatography (silica, EtOAc/EtOH, 1:1). Yield 0.68 g (98%) of orange foam. HR-MS (TOF ES+): *m*/*z* exp. 825.3280 and calcd. 825.3274 for [M + H]$^+$; ^{1}H NMR ([D_6]-DMSO), max./min. where observed: δ = 8.49–8.46 (m, 4 H, $H_{Py-2,6}$), 8.04–8.00/7.88–7.85 (m, 2 H, H_{NH}), 7.27/7.21 (d, *J* = 5.0 Hz, 4 H, $H_{Py-3,5}$), 4.73–4.69 (m, 4 H, $H_{Fc-\alpha}$), 4.32–4.29 (m, 4 H, $H_{Fc-\beta}$), 4.00 (s, 2 H, $H_{Py-\alpha}$), 3.89 (s, 2 H, $H_{Py-\alpha}$), 3.68–3.12 (m, 12 H, H_{Bb}), 1.38/1.41 (s, 18 H, H_{OtBu}), max./min. ratio 64:36.

Re^I Complexes 3_{Re}–6_{Re}, General Procedure: $Re(CO)_5Cl$ and the corresponding ferrocenoyl peptide **3**–**6** were suspended in chloroform and refluxed overnight.[10] The reaction mixture was cooled to room temperature, evaporated to a small volume. The compounds were then purified through column chromatography using an

dichloromethane/methanol gradient (0 to 5%). The rhenium complexes $\mathbf{3_{Re}}$–$\mathbf{6_{Re}}$ were stored in the dark.

[{Fe[C_5H_4-CO-aeg(dpa-ph)-O*t*Bu][C_5H_5]}Re(CO)$_3$Cl] ($\mathbf{3_{Re}}$): Re(CO)$_5$Cl (22 mg, 0.06 mmol), **3** (39.8 mg, 0.06 mmol) and chloroform (30 mL) were reacted. Yield 23.8 mg (59.1%), orange solid. HR-MS (TOF ES+): *m*/*z* exp. 964.1339 and calcd. 964.1287 for $[C_{39}H_{38}ClFeN_5O_7{}^{185}Re]^+$; ^{1}H NMR ([D$_6$]DMSO), max./min. where observed: δ = 8.82–8.79 (m, 2 H, $H_{py\text{-}6}$), 8.20–8.13 (m, 2 H, $H_{py\text{-}4}$), 7.85/7.92 (br. s, 1 H, H_{NH}), 7.67/7.77 (d, J = 8.3 Hz, 2 H, $H_{ph\text{-}3,5}$), 7.60–7.30 (m, 6 H, $H_{ph\text{-}2,6}$, $H_{py\text{-}3}$ and $H_{py\text{-}5}$), 4.69/4.76 (br. s, 2 H, $H_{Fc\text{-}\alpha}$), 4.33–4.31 (m, 2 H, $H_{Fc\text{-}\beta}$), 4.16/4.08 (s, 5 H, $Fc_{unsubst.}$), 4.06–4.00 (m, 2 H, $H_{Bb\text{-}5}$), 3.62–3.35 (m, 4 H, $H_{Bb\text{-}2}$ and $H_{Bb\text{-}3}$), 1.45/1.33 (s, 9 H, H_{OtBu}), max./min. ratio 59:41. IR (KBr): $\tilde{\nu}$ = 3357, 3084, 2978, 2933, 2019, 1908, 1896, 1736, 1644, 1601, 1528, 1479, 1464, 1431, 1368, 1320, 1283, 1242, 1154 cm^{-1}.

[{Fe[C_5H_4-CO-aeg(dpa-ph)-O*t*Bu]$_2$}{Re(CO)$_3$Cl}$_2$] ($\mathbf{4_{Re}}$): Re(CO)$_5$Cl (25 mg, 0.07 mmol), **4** (57 mg, 0.04 mmol) and chloroform (30 mL) were used. Yield 31.2 mg (52.8%), orange solid. HR-MS (TOF ES+): *m*/*z* exp. 1745.2523 and calcd. 1745.2589 for [M + H]$^+$; ^{1}H NMR ([D$_6$]DMSO), max./min. where observed: δ = 8.80 (br. s, 2 H, $H_{Py\text{-}6}$), 8.17–8.12 (m, 2 H, $H_{Py\text{-}4}$), 8.01–7.89 (br. s, 1 H, H_{NH}), 7.65/7.75 (d, J = 8.3 Hz, 2 H, $H_{ph\text{-}3,5}$), 7.57–7.32 (m, 6 H, $H_{ph\text{-}2,6}$, $H_{py\text{-}3}$ and $H_{py\text{-}5}$), 4.71–4.62 (m, 4 H, $H_{Fc\text{-}\alpha}$), 4.29–4.02 (m, 8 H, $H_{Fc\text{-}\beta}$ and $H_{Bb\text{-}5}$), 3.60–3.41 (m, 4 H, $H_{Bb\text{-}2}$ and $H_{Bb\text{-}3}$), 1.44/1.30 (s, 9 H, H_{OtBu}), max./min. ratio 57:43. IR (KBr): $\tilde{\nu}$ = 3365, 3085, 2978, 2932, 2019, 1914, 1898, 1735, 1644, 1612, 1533, 1513, 1479, 1465, 1434, 1313, 1282, 1228, 1197, 1153 cm^{-1}.

[{Fe[C_5H_4-CO-aeg(py)-O*t*Bu][C_5H_5]}$_2$Re(CO)$_3$Cl] ($\mathbf{5_{Re}}$): Re(CO)$_5$Cl (66 mg, 0.18 mmol), **5** (151 mg, 0.30 mmol) and chloroform (30 mL) were used. Yield 127 mg (64.7%), orange solid. HR-MS (TOF ES+): *m*/*z* exp. 1317.2500 and calcd. 1317.2448 for [M + H]$^+$; ^{1}H NMR ([D$_6$]DMSO), max./min. where observed: δ = 8.57 (br. s, 4 H, $H_{Py\text{-}2,6}$), 7.95/7.78 (br. s, 2 H, H_{NH}), 7.44–7.40 (m, 4 H, $H_{Py\text{-}3,5}$), 4.75/4.72 (br. s, 4 H, $H_{Fc\text{-}\alpha}$), 4.35/4.33 (br. s, 4 H, $H_{Fc\text{-}\beta}$), 4.14 (s, 5 H, $Fc_{unsubst.}$), 4.00/4.30 (s, 4 H, $H_{py\text{-}\alpha}$), 4.00/3.77 (s, 4 H, $H_{Bb\text{-}5}$), 3.53–3.38 (m, 8 H, $H_{Bb\text{-}2}$ and $H_{Bb\text{-}3}$), 1.37/1.41 (s, 18 H, H_{OtBu}), max./min. ratio 67:33. IR (KBr): $\tilde{\nu}$ = 3354, 3095, 2979, 2934, 2021, 1913, 1886, 1737, 1649, 1529, 1452, 1429, 1368, 1291, 1232, 1155 cm^{-1}.

[{Fe[C_5H_4-CO-aeg(py)-O*t*Bu]$_2$}Re(CO)$_3$Cl] ($\mathbf{6_{Re}}$): Re(CO)$_5$Cl (26 mg, 0.07 mmol), **6** (60 mg, 0.07 mmol) and chloroform (30 mL) were reacted. Yield 52.5 mg (63.9%), orange solid. HR-MS (TOF ES+): *m*/*z* exp 1131.2368 and calcd. 1131.2330 for [M + H]$^+$; ^{1}H NMR ([D$_6$]DMSO), max./min. where observed: δ = 8.45–8.42/8.36–8.35 (m, 4 H, $H_{Py\text{-}2,6}$), 8.06–7.97/8.65–8.56 (m, 2 H, H_{NH}), 7.33–7.30/7.23–7.22 (m, 4 H, $H_{Py\text{-}3,5}$), 4.67/4.61/4.56 (br. s, 4 H, $H_{Fc\text{-}\alpha}$), 4.13/4.18 (br. s, 4 H, $H_{Fc\text{-}\beta}$), 4.04–3.76/4.24 (m and s, 12 H, $H_{Py\text{-}a}$, $H_{Bb\text{-}5}$ and $H_{Bb\text{-}2}$) 3.57–3.44 (m, 4 H, $H_{Bb\text{-}3}$), 1.39/1.46 (s, 18 H, H_{OtBu}) ppm. IR (KBr): $\tilde{\nu}$ = 3353, 3091, 2979, 2930, 2021, 1912, 1885, 1738, 1656, 1529, 1458, 1429, 1369, 1291, 1231, 1153 cm^{-1}.

Supporting Information (see also the footnote on the first page of this article): Example NMR spectra and FTIR spectra.

Acknowledgments

We are grateful to the National Science Foundation (NSF) (CHE – 0718373) and the David and Lucile Packard Foundation for generous support of this work. Mass spectra were collected with the assistance of the Penn State Huck Institutes for the Life Sciences Mass Spectrometry Facility.

[1] For a detailed literature review, see A. Togni, T. Hayashi, *Ferrocenes: homogeneous catalysis, organic synthesis, materials science*, VCH Verlagsgesellschaft, Weinheim, Germany, **1995**; A. Togni, R. L. Halterman, *Metallocenes: Synthesis-Reactivity Applications*, Wiley-VCH, Weinheim, Germany, **1998**.

[2] For a comprehensive overview of ferrocene and other metallocene chemistry, see N. J. Long, *Metallocenes: An Introduction to Sandwich Complexes*, Blackwell Science, **1998**.

[3] a) V. C. Gibson, N. J. Long, A. J. P. White, C. K. Williams, D. J. Williams, *Organometallics* **2000**, *19*, 4425–4428; b) C.-J. Fang, C.-Y. Duan, H. Mo, C. He, Q.-J. Meng, Y.-J. Liu, Y.-H. Mei, Z.-M. Wang, *Organometallics* **2001**, *20*, 2525–2532; c) G. Li, Y. Song, H. Hou, L. Li, Y. Fan, Y. Zhu, X. Meng, L. Mi, *Inorg. Chem.* **2003**, *42*, 913–920; d) R. C. J. Atkinson, V. C. Gibson, N. J. Long, *Chem. Soc. Rev.* **2004**, *33*, 313–328; e) X. Meng, H. Hou, G. Li, B. Ye, T. Ge, Y. Fan, Y. Zhu, H. Sakiyama, *J. Organomet. Chem.* **2004**, *689*, 1218–1229; f) Y. Gao, B. Twamley, J. N. M. Shreeve, *Organometallics* **2006**, *25*, 3364–3369; g) Y. Yamaguchi, W. Ding, C. T. Sanderson, M. L. Borden, M. J. Morgan, C. Kutal, *Coord. Chem. Rev.* **2007**, *251*, 515–524.

[4] a) S. Fukuzumi, *Bull. Chem. Soc. Jpn.* **2006**, *79*, 177–195; b) D. Gonzalez-Rodriguez, T. Torres, M. Olmstead Marilyn, J. Rivera, A. Herranz Maria, L. Echegoyen, A. Castellanos Carmen, M. Guldi Dirk, *J. Am. Chem. Soc.* **2006**, *128*, 10680–10681; c) J. Yuasa, S. Yamada, S. Fukuzumi, *J. Am. Chem. Soc.* **2008**, *130*, 5808–5820.

[5] a) L. Wilputte-Steinert, *J. Mol. Catal.* **1978**, *4*, 113–123; b) R. M. Lahtinen, D. J. Fermin, H. Jensen, K. Kontturi, H. H. Girault, *Electrochem. Commun.* **2000**, *2*, 230–234.

[6] See for example: a) K. Tanaka, M. Shionoya, *J. Org. Chem.* **1999**, *64*, 5002–5003; b) S. Atwell, E. Meggers, G. Spraggon, P. G. Schultz, *J. Am. Chem. Soc.* **2001**, *123*, 12364–12367; c) H. Weizman, Y. Tor, *Chem. Commun.* **2001**, 453–454; d) K. Tanaka, A. Tengeiji, T. Kato, N. Toyama, M. Shionoya, *Science* **2003**, *299*, 1212–1213; e) L. Zhang, E. Meggers, *J. Am. Chem. Soc.* **2005**, *127*, 74–75; f) A. Kuesel, J. Zhang, M. A. Gil, A. C. Stueckl, W. Meyer-Klaucke, F. Meyer, U. Diederichsen, *Eur. J. Inorg. Chem.* **2005**, 4317–4324; g) S. J. Kim, E. T. Kool, *J. Am. Chem. Soc.* **2006**, *128*, 6164–6171; h) R. M. Franzini, R. M. Watson, G. K. Patra, R. M. Breece, D. L. Tierney, M. P. Hendrich, C. Achim, *Inorg. Chem.* **2006**, *45*, 9798–9811; i) K. Tanaka, G. H. Clever, Y. Takezawa, Y. Yamada, C. Kaul, M. Shionoya, T. Carell, *Nat. Nanotechnol.* **2006**, *1*, 190–194; j) D. Shin, C. Switzer, *Chem. Commun.* **2007**, 4401–4403; k) D. Böhme, N. Düpre, D. A. Megger, J. Müller, *Inorg. Chem.* **2007**, *46*, 10114–10119.

[7] a) B. P. Gilmartin, K. Ohr, R. L. McLaughlin, R. Koerner, M. E. Williams, *J. Am. Chem. Soc.* **2005**, *127*, 9546–9555; b) K. Ohr, B. P. Gilmartin, M. E. Williams, *Inorg. Chem.* **2005**, *44*, 7876–7885; c) B. P. Gilmartin, R. L. McLaughlin, M. E. Williams, *Chem. Mater.* **2005**, *17*, 5446–5454; d) K. Ohr, R. L. McLaughlin, M. E. Williams, *Inorg. Chem.* **2007**, *46*, 965–974; e) L. A. Levine, H. Youm, H. P. Yennawar, M. E. Williams, *Eur. J. Inorg. Chem.* **2008**, *26*, 4083–4091.

[8] C. P. Myers, B. P. Gilmartin, M. E. Williams, *Inorg. Chem.* **2008**, *47*, 6738–6747.

[9] a) P. A. Anderson, F. R. Keene, E. Horn, E. R. T. Tiekink, *Appl. Organomet. Chem.* **1990**, *4*, 523–533; b) R. V. Slone, K. D. Benkstein, S. Belanger, J. T. Hupp, I. A. Guzei, A. L. Rheingold, *Coord. Chem. Rev.* **1998**, *171*, 221–243; c) S. J. Lee, J. T. Hupp, *Coord. Chem. Rev.* **2006**, *250*, 1710–1723.

[10] S. J. A. Pope, B. J. Coe, S. Faulkner, *Chem. Commun.* **2004**, 1550–1551.

[11] a) For IR patterns of M(CO), M(CO)$_2$ and M(CO)$_3$ fragments see: G. R. Stephenson in *Bioorganometallics: Biomolecules, Labeling, Medicine* (Ed.: G. Jaouen), Wiley-VCH, Weinheim, Germany, **2006**, pp. 215–265; b) for IR patterns of the *mer*- and *fac*-Re(CO)$_3$ fragments see for example: S. Sato, T. Morimoto, O. Ishitani, *Inorg. Chem.* **2007**, *46*, 9051–9053.

[12] a) T. Moriuchi, A. Nomoto, K. Yoshida, A. Ogawa, T. Hirao, *J. Am. Chem. Soc.* **2001**, *123*, 68–75; b) S. I. Kirin, H.-B. Kraatz, N. Metzler-Nolte, *Chem. Soc. Rev.* **2006**, *35*, 348–354; c) L. Barišić, M. Čakić, K. A. Mahmoud, Y.-N. Liu, H.-B. Kraatz, H. Pritzkow, S. I. Kirin, N. Metzler-Nolte, V. Rapić, *Chem. Eur. J.* **2006**, *12*, 4965–4980.
[13] a) Y. Jin, K. Tonan, S. Ikawa, *Spectrochim. Acta Part A* **2002**, *58*, 2795–2802; b) J. Lapić, D. Siebler, K. Heinze, V. Rapić, *Eur. J. Inorg. Chem.* **2007**, *14*, 2014–2024.
[14] D. R. Scott, R. S. Becker, *J. Chem. Phys.* **1961**, *35*, 516–531.
[15] a) Y.-S. Yang, Y.-D. Lin, Y.-H. Lin, F.-L. Liao, *J. Org. Chem.* **2004**, *69*, 3517–3525; b) S.-L. Zheng, X.-M. Chen, *Aust. J. Chem.* **2004**, *57*, 703–712; c) D. E. Morris, Y. Ohsawa, D. P. Segers, M. K. DeArmond, K. W. Hanck, *Inorg. Chem.* **1984**, *23*, 3010–3017; d) C. Seward, J. Pang, S. Wang, *Eur. J. Inorg. Chem.* **2002**, 1390–1399.
[16] N. M. Shavaleev, A. Barbieri, Z. R. Bell, M. D. Ward, F. Barigelletti, *New J. Chem.* **2004**, *28*, 398–405.
[17] R. Martínez, I. Ratera, A. Tárraga, P. Molina, J. Veciana, *Chem. Commun.* **2006**, 3809–3811.
[18] A. J. Bard, L. R. Faulkners, *Electrochemical Methods, Fundamentals and Applications*, 2nd ed., John Wiley & Sons, New York, **2001**.
[19] K. Bushell, C. Gialou, C. H. Goh, N. J. Long, J. Martin, A. J. P. White, C. K. Williams, D. J. Williams, M. Fontani, P. Zanello, *J. Organomet. Chem.* **2001**, *637–639*, 418–425.
[20] a) J.-C. Moutet, E. Saint-Aman, G. Royal, S. Tingry, R. Ziessel, *Eur. J. Inorg. Chem.* **2002**, 692–698; b) A. Ion, M. Buda, J.-C. Moutet, E. Saint-Aman, G. Royal, I. Gautier-Luneau, M. Bonin, R. Ziessel, *Eur. J. Inorg. Chem.* **2002**, 1357–1366; c) F. E. Appoh, D. S. Thomas, H.-B. Kraatz, *Macromolecules* **2006**, *39*, 5629–5638.
[21] a) D. L. Reger, K. J. Brown, J. R. Gardinier, M. D. Smith, *J. Organomet. Chem.* **2005**, *690*, 1889–1900; b) M. P. Juliarena, G. T. Ruiz, E. Wolcan, R. O. Lezna, M. R. Feliz, G. Ferraudi, J. Guerrero, *Organometallics* **2007**, *26*, 272–280.
[22] A. Atkins, J. de Paula, *Physical Chemistry*, 7th ed., Freeman, New York, **2002**.
[23] J. Cavanagh, W. J. Fairbrother, A. G. Palmer III, M. Rance, N. J. Skelton, *Protein NMR Spectroscopy Principles and Practice*, 2nd ed, Academic Press, Burlington, MA, **2007**.
[24] J. Brooks, Y. Babayan, S. Lamansky, P. I. Djurovich, I. Tsyba, R. Bau, M. E. Thompson, *Inorg. Chem.* **2002**, *41*, 3055–3066.
[25] A. P. Krapcho, C. S. Kuell, *Synth. Commun.* **1990**, *20*, 2559–2564.
[26] S. I. Kirin, H. P. Yennawar, M. E. Williams, *Eur. J. Inorg. Chem.* **2007**, 3686–3694.

Received: August 29, 2008
Published Online: January 14, 2009

